Available online at www.sciencedirect.com

ScienceDirect

Procedia CIRP 45 (2016) 291 – 294

www.elsevier.com/locate/procedia

3rd CIRP Conference on Surface Integrity (CIRP CSI)

Prediction of the Principal Stress Direction for 5-axis Ball End Milling

V. Böß[a], T. Grove[a], B. Denkena[a], A. Mücke[a,*], D. Nespor[a]

[a]*Institute of Production Engineering and Machine Tools (IFW), Leibniz Universität Hannover, An der Universität 2, 30823 Garbsen*

* Corresponding author. Tel.: +49-511-762-18270; fax: +49-511-762-5115. *E-mail address:* Muecke@ifw.uni-hannover.de

Abstract

While regenerating damaged components, e.g. compressor blades, the removal of excess weld material called re-contouring often determines the surface integrity including the residual stress state. A load-specific residual stress state is beneficial for lifetime. This leads to the necessity to predict the resulting residual stress state after machining. The paper describes two models, which predict the principal stress direction as a residual stress characteristic for 5-axis ball nose end milling of Ti-6Al-4V. One model uses process force components, the other is based on the microtopography of the workpiece, which is influenced by the kinematics of the process.

Peer-review under responsibility of the scientific committee of the 3rd CIRP Conference on Surface Integrity (CIRP CSI)

Keywords: Milling, Residual Stress, Principal Stress Direction, Titanium

1. Introduction

In the sector of aviation, an important source of revenue are aftermarket services, where repair represents 67 % of the total revenue in the field of maintenance, repair and overhaul (MRO) [1]. As an example, economical repair processes for compressor or turbine blades are crucial to reduce life cycle costs [2]. The increasing usage of Blade Integrated Disks (BLISKs), where blades and disk are made out of one single workpiece, offer advantages e.g. in weight reduction, although raising the repairing process degree of complexity and need for cost effectiveness. Therefore, it is necessary to investigate such processes in terms of economy and effects on the refurbished product.

The process chain of blade repair consists of four phases: pre-treatment, material deposit, re-contouring and post-treatment [3]. The pre-treatment incorporates de-coating, cleaning, inspection and measurement, whereas the material deposit can be accomplished by built-up or patch welding and filling cracks through brazing [2]. The re-contouring is done either manually or automatically via cutting. If no further post-treatment is applied, it determines the final surface integrity, including the residual stress state after machining, which has a major impact on fatigue life [4], [5]. In this paper, due to the sustained growth of BLISK usage, which have a complex shape, the process of ball end milling will be examined. They are commonly made of titanium, wherefore Ti-6Al-4V will be considered.

There is only limited knowledge concerning machining induced residual stresses of repaired parts. To expand the research field of re-contouring dealing with residual stress formation, Denkena et al. investigated the residual stresses after ball end milling of welded Ti-6Al-4V (abbr. Ti64) parts [3]. They identified the most significant parameters on the amount of residual stresses, namely the cutting edge radius r_β, cutting strategy (up/down cut) and feed per tooth f_z. It is also shown that thermal induced residual stresses can be neglected in the investigated parameter field. The temperatures during re-contouring seldom exceed $T_{crit,Ti64}$ = 480°C, at which the comparative stress equals the yield strength and tensile residual stress may occur according to [3]. Furthermore, they introduce the term “surface generating forces”, which considers the cross section generating the final surface during cutting. The surface generating forces are used to explain the mechanical effects of residual stresses for re-contouring and will be applied in this paper. A detailed explanation of the surface generating forces is given in [3].

Peer-review under responsibility of the scientific committee of the 3rd CIRP Conference on Surface Integrity (CIRP CSI)
doi:10.1016/j.procir.2016.02.145

Besides the amount of residual stress, compressive or tensile, the principal stress direction is needed to fully characterize the residual stress state and it has an effect e.g. on crack propagation. This leads to the necessity to predict the principal stress direction, which is the aim of this paper.

While the principal stress direction correlates with the direction of primary motion during planing [6] and face grinding [7], this can be different for processes with more complex kinematics. For orthogonal turning, Jacobus et al. showed that the tool cutting edge inclination δ correlates with the principal stress direction while the cutting speed v_c does not during an oblique cutting operation. This is represented through the coordinate system X', Y', Z' in Fig. 1, which is in line with σ_1 and σ_2. The principal stress direction of σ_1 is more aligned with the direction of the resulting force vector from F_{cN} and F_c. These findings are expanded upon the prediction of the principal stress direction during ball nose end milling.

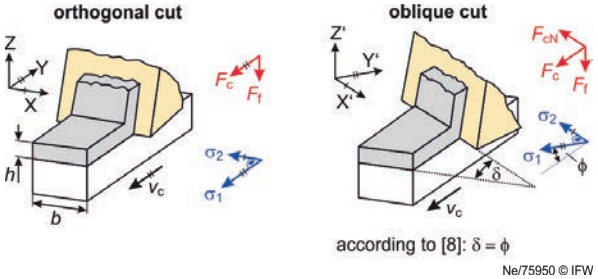

Fig. 1. Correlation between principal stress direction and forces according [8]

2. Workflow and experimental setup

Ti64 parts were re-contoured on a Deckel Maho DMU 125P using a 10 mm ball end mill type Seco JH970100 to identify the significant factors influencing the principal stress direction. Therefore, residual stress measurements were executed via X-Ray diffraction using a General Electric XRD 3003 TT diffractometer to calculate the principal stresses and their direction ϕ with equation 1, 2 and 3 according to [9]. The corresponding experiments will be detailed in section 3.

$$\sigma_1 = \frac{\sigma_{90°} - \sigma_{0°} \cdot cot\phi^2}{1 - cot\phi^2} \quad (1)$$

$$\sigma_2 = \frac{\sigma_{90°} - \sigma_{0°} \cdot tan\phi^2}{1 - tan\phi^2} \quad (2)$$

$$\phi = \frac{1}{2}\arctan\left(\frac{\sigma_{0°} + \sigma_{90°} - 2 \cdot \sigma_{45°}}{\sigma_{0°} - \sigma_{90°}}\right) \quad (3)$$

The principal stress states obtained are used as a reference to judge the capability of the models predicting the principal stress direction. They will be introduced in section 4 and compared in section 5. Finally, a conclusion will be drawn in section 6.

3. Identification of factors influencing the principal stress direction while ball nose end milling of Ti-6Al-4V

Due to the complex kinematic of 5-axis ball end milling, the significant factors determining the principal stress direction need to be identified experimentally, which is done in this section. Therefore, the main process parameters of 5-axis ball end milling will be described first.

The additional degrees of freedom enable the tool to lean in different directions. This is characterized through lead angle λ and tilt angle τ. The lead angle λ is positive, if the cutting tool is sloped in feed direction, referred to as draw-cutting. For negative λ, the cut is referred to as drill-cut. During drill-cut, the tip of the tool may be in engagement with the workpiece but this is usually avoided because of increased process forces, ploughing, tool wear and surface blemishes. The cutting tool is sloped in the direction of uncut surface for positive tilt angles τ. Due to the ball end, the cutting speed v_c varies along the cutting edge. Therefore the mean cutting speed $v_{c,m}$ is used, based on the cutting edge angle κ, which is valid for the surface generated and described in [3].

A fractional factorial experimental design has been set up to classify the most significant parameters (tool geometry and process parameters) on the principal stress direction. Table 1 lists the factor combinations (screening design), which were chosen to provide stability of the process, prevent tool breakage and to meet the quality requirements for re-contouring high valuable goods in their tolerance field to guarantee the validity of significance.

Table 1. Factor combinations for fractional factorial design.

Factor	-	+
Mean cutting speed $v_{c,m}$ [m/min]	15	60
Feed per tooth f_z [mm]	0.15	0.4
Depth of cut a_p [mm]	0.4	1.0
Step over b_r [mm]	0.2	0.5
Lead angle λ [°]	15	60
Tilt angle τ [°]	0	60
Cutting strategy	Up-cut	Down-cut
Clearance angle α [°]	6	12
Rake angle γ [°]	8	14
Edge radius r_β [µm]	4	30

Each experiment is repeated once (n = 2). The experiments result in 64 variances of 32 combinations for the high (+) and low (-) factors. All effects e of each factor are calculated with

$$e = \frac{1}{32}\sum_{i=1}^{32}\overline{x_i}^{(+)} - \frac{1}{32}\sum_{j=1}^{32}\overline{x_j}^{(-)} \quad (4)$$

where the mean values are $\overline{x_i}^{(+)}$ and $\overline{x_j}^{(-)}$ for all high and low combinations respectively. A student distribution has been used to determine the significance of an effect with a probability of s = 99.5 %. Random effects such as scattered values of X-Ray diffraction limit the significance. In Fig. 2, the effects of the fractional factorial design are shown. It can be seen that lead and tilt angle are the most significant factors. For all other factors, the principal stress direction almost corresponds to the machining direction. The high limits of significance are a result of the Gaussian error propagation, because the squared values of the uncertainties of Eq. 1, 2 and 3 add up. Thus, small fluctuations of the three residual stress measurements lead to high variations of the principal stress

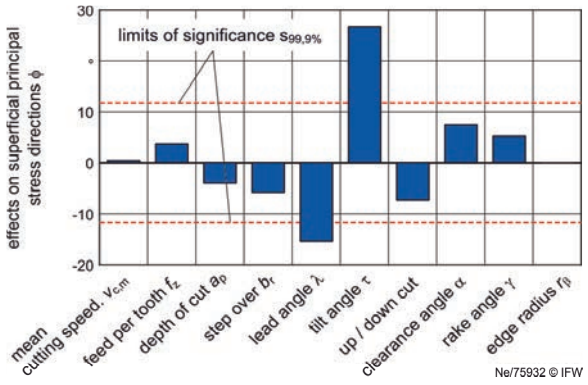

Fig. 2. Result of the fractional factorial design

directions. Lead and tilt angle show an interdependency, but the exact interaction among each other is unknown, wherefore a CCD plan has been performed according to table 2.

Table 2. Factor combinations of CCD plan for identifying interdepencies

Factor	variations				
Lead angle λ [Deg.]	0	8.8	30.0	51.2	60.0
Tilt angle τ [Deg.]	0	8.8	30.0	51.2	60,0
(standardized)	$-\sqrt{2}$	-1	0	1	$\sqrt{2}$

The factors show nonlinear interactions as the regression of the measured data (R^2_{corr} = 0.65, normally distributed residuals) depicts in Fig. 3. Using small lead angles λ and high tilt angles τ simultaneously, the principal direction ϕ changes to positive values, while raising λ leads to a tendency of negative angles ϕ. Small tilt angles τ reverse the described effect. The strong interdepency can be explained physically by the cutting

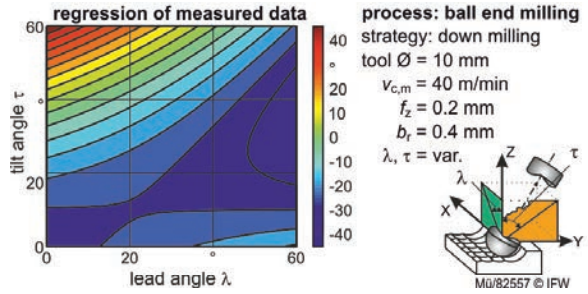

Fig. 3. Regression of measured data, interdepency between λ and τ

direction of the tool. λ and τ change the cutting direction and thus the surface generation, which will be underlined by the presented models in the upcoming section 4.

4. Models predicting the principal stress direction

In order to extend the knowledge concerning the residual stress state of ball end milled Ti64 goods, the theory of the two models to predict the principal stress direction is presented in this section. The results of both models are shown in section 5.

4.1. Prediction of the principal stress direction through process forces

Jacobus et al. showed that during orthogonal and oblique cutting, the principal stress direction is determined by tool orientation. These findings are transferred to ball end milling and it is proposed, that a correlation between the principal stress direction and the direction of the surface generating forces as explained in [3] exists. Thus, only forces will be considered, which act on the surface during the final cut. Figure 4 shows a simulated surface including the infinitesimal surface generating vector field, feed vector $\vec{v}_f$ and the surface normal vector $\vec{n}$. It is derived from a material removal simulation performed with the approach of Boess et al. and the software

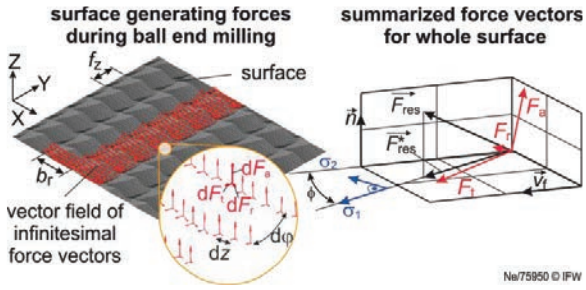

Fig. 4. Surface generating forces during ball end milling and summarized force vectors

platform CutS [10]. All infinitesimal surface generating force vectors of the chosen surface area are summarized to the resulting force vector $\overrightarrow{F_{res}}$. This is comparable with a residual stress measurement that is, depending on the collimator and specimen tilt, an integral mean value [11]. Only the force components of $\overrightarrow{F_{res}}$ are considered, which are orthogonal to the surface normal vector $\vec{n}$ and thus analogous to $\sigma_z = 0$. The result is the projected force vector $\overrightarrow{F^*}_{res} = \vec{F}_{res} - \langle \vec{F}_{res}, \vec{n} \rangle \cdot \vec{n}$. It leads to the functional relation to predict the principal stress direction:

$$\phi = \begin{cases} \arctan\left(\frac{\langle \vec{n}, \vec{v_f}, \overrightarrow{F^*_{res}} \rangle}{\langle \vec{v_f}, \overrightarrow{F^*_{res}} \rangle}\right) & -45° \leq \arctan\left(\frac{\langle \vec{n}, \vec{v_f}, \overrightarrow{F^*_{res}} \rangle}{\langle \vec{v_f}, \overrightarrow{F^*_{res}} \rangle}\right) \leq 45°; \\ -\arctan\left(\frac{\langle \vec{v_f}, \overrightarrow{F^*_{res}} \rangle}{\langle \vec{n}, \vec{v_f}, \overrightarrow{F^*_{res}} \rangle}\right) & -45° > \arctan\left(\frac{\langle \vec{n}, \vec{v_f}, \overrightarrow{F^*_{res}} \rangle}{\langle \vec{v_f}, \overrightarrow{F^*_{res}} \rangle}\right) > 45°; \end{cases} \quad (5)$$

$\langle \vec{n}, \vec{v_f}, \overrightarrow{F^*_{res}} \rangle$ is the triple product and $\langle \vec{v_f}, \overrightarrow{F^*_{res}} \rangle$ denotes the scalar product. This defines a right-handed coordinate system with the axis of rotation $\vec{n}$. If $\overrightarrow{F_{res}}$ points in direction of $\vec{v}_f$, the triple and scalar product are zero, the principal stress direction equals the feed direction and then one has $\phi = 0°$. Equation 5 consists of two ranges of values. For -45° to 45° the upper part is valid, else the lower, thus Eq. 5 has the same range as Eq. 4. Equation 5 always represents the direction of the largest absolute principal stress value.

4.2. Prediction of the principal stress direction through micro topography of the workpiece

The second model predicts the principal stress direction depending on the resultant microtopography of the workpiece due to machining. Amongst others, the grinding marks of a tool have an effect on the surface, especially when the tool is considered to be sharp and there is only a small cutting edge

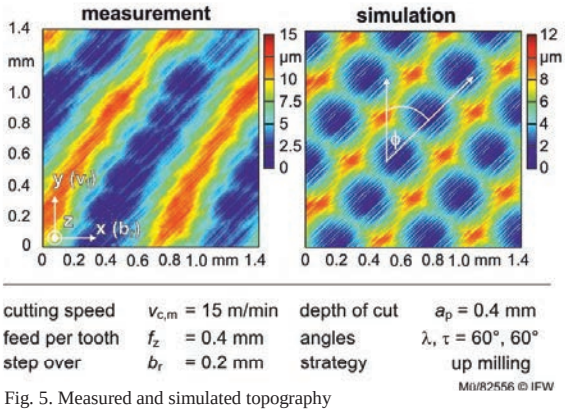

Fig. 5. Measured and simulated topography

rounding. During machining, this chipping is mapped onto the surface as a negative and it is used to predict the principal stress direction. Its effect can be seen in Fig. 5 in which a measured and simulated surface including chipping and radial deviation, similar performed to [12], are compared. Direction y correlates with feed direction and x with step over b_r. The angle is measured between the direction of strain indicated through the chipping and a line in direction of feed motion. It is proposed that this angle equals the principal stress direction ϕ.

5. Results

The simulated principal stress directions derived from Eq. 5 (model 1) as well as model 2 are compared with the experimental results in Fig. 6. It can be seen that Eq. 5 predicts the tendencies of the angles correctly, although high deviations up to $\Delta\phi_{max} = 23.4°$ occur. This is due to the high variance of the measurements represented through error bars in Fig. 6. The second model represents the principal stress direction ϕ similar to model 1 and it shows that the principal stress direction ϕ can be predicted via the texture of the final generated surface, which is determined by the kinematic of the process. Both models over- and underestimate the angle ϕ and there is no tendency visible whether model 1 or model 2 should be preferred. Amongst others, the included force and material simulations, which are simplified approaches as well, influence the accuracy of both models.

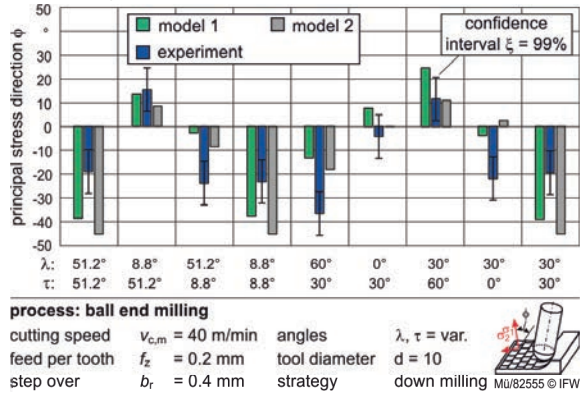

Fig. 6. Comparison of measured and predicted principal stress direction

6. Conclusion

The most relevant parameters affecting the principal stress direction while ball end milling Ti64 have been identified experimentally. It can be summarized that only the tool angles λ and τ have a significant influence on the principal stress direction due to their impact on the surface generating forces and resulting texture of the generated surface. However, their interdependency is nonlinear.

Furthermore, two models have been presented to predict the principal stress direction. They are both based on material removal simulations and their prognosis is in a good agreement with the experimental measured principal stress directions. Comparing practicability, model 2 is easier to use if compared to model 1, because no force simulation is needed and the surface generating forces do not have to be calculated. Although the tools have to be modelled properly to simulate the chipping correctly, which can be time consuming.

Acknowledgements

The authors thank the German Research Foundation (DFG) for the financial support within the Collaborative Research Centre 871: Refurbishment of complex capital goods.

References

[1] Uhlmann, E., Röhner, M., Baumgarten, J., van Duikeren, B., 2011, Markt- und Trendstudie Maintenance, Repair and Overhaul, Fraunhofer Institut Produktionsanlagen und Konstruktionstechnik.

[2] Eberlein, A., 2007, Phases of High-Tech Repair Implementation, 18th International Symposium on Airbreathing Engines (ISABE) (Beijing).

[3] Denkena, B., Nespor, D., Böß, V., Köhler, J., 2014, Residual stresses formation after re-contouring of welded Ti-6Al-4V parts by means of 5-axis ball nose end milling, CIRP Journal of Manufacturing Science and Technology, 7:347-360.

[4] Brinksmeier, E., Cammett, J., König, W., 1982, Residual Stresses – Measurement and Causes in Machining Processes, Annals of the CIRP, 31:491–510.

[5] Ulutan, D., Ozel, T., 2011, Machining Induced Surface Integrity in Titanium and Nickel Alloys: A Review, International Journal of Machine Tools & Manufacture, 51:250–280.

[6] Tönshoff, H.K., 1966, Eigenspannungen und plastische Verformungen im Werkstück durch spanende Bearbeitung, Dr.-Ing. Dissertation, Technische Hochschule Hannover.

[7] Brinksmeier, E., 1982, Randzonenanalyse geschliffener Werkstücke, Dr.-Ing. Dissertation, Universität Hannover.

[8] Jacobus, K., DeVor R.E., Kapoor, S.G., 2000, Machining-Induced Residual Stress: Experimentation and Modeling, Journal of Manufacturing Science and Engineering, 122:20-31.

[9] Macherauch, E., Müller, P., 1961, Das $\sin^2\psi$-Verfahren der röntgenografischen Spannungsmessung. Zeitschrift für angewandte Physik 7, pp. 305-312.

[10] Böß, V., Nespor, D., Samp, A., Denkena, B., 2013, Numerical Simulation of Process Forces During Re-contouring of Welded Parts Considering Different Material Properties, CIRP Journal of Manufacturing Science and Technology, 6/3:167-1.

[11] Plöger, J. M., 2002, Randzonenbeeinflußung durch Hochgeschwindigkeitsdrehen, Dr.-Ing. Dissertation, Universität Hannover.

[12] Nespor, D., Denkena, B., Grove, T., Pape, O., 2015, Surface topography after re-contouring of welded Ti-6Al-4V parts by means of 5-axis ball nose end milling. The International Journal of Advanced Manufacturing Technology, pp. 1-18.